Molecular Crystals and Liquid Crystals

ISSN: 1542-1406 (Print) 1563-5287 (Online) Journal homepage: http://www.tandfonline.com/loi/gmcl20

Nicotinamide–Indole Binary Drug System: Thermodynamic and Interfacial Studies

Vishnu Kant

To cite this article: Vishnu Kant (2015) Nicotinamide–Indole Binary Drug System: Thermodynamic and Interfacial Studies, Molecular Crystals and Liquid Crystals, 608:1, 211-222, DOI: 10.1080/15421406.2014.963278

To link to this article: http://dx.doi.org/10.1080/15421406.2014.963278

Mol. Cryst. Liq. Cryst., Vol. 608: pp. 211–222, 2015

ISSN: 1542-1406 print/1563-5287 online
DOI: 10.1080/15421406.2014.963278

Nicotinamide–Indole Binary Drug System: Thermodynamic and Interfacial Studies

VISHNU KANT*

Department of Chemistry, V. K. S. University, Ara, Bihar, India

Crystal engineering, which can potentially be applied to a wide range of crystalline materials, offer an alternative and potentially fruitful method for improving pharmaceutical properties of drugs. The molecular mobility inherent to amorphous/crystalline phases can lead to molecular associations between different components, such that a single crystalline phase of multiple components is formed. The present investigation measures the solid–liquid equilibria (SLE) of nicotinamide (NA)-indole (IN) binary drug system. The solid–liquid equilibrium phase diagram of NA-IN system was determined by the thaw-melt method in the form of a temperature-composition curve. It shows the formation of a simple eutectic at a 0.953 mole fraction of indole, at 48°C. The excess thermodynamic quantities (g^E, h^E, and s^E) have been estimated by computing heat of fusion data and activity coefficient of the component in a binary mix. These values highlight the ordering, stability, and structure of eutectic and non-eutectic alloys. The thermodynamic mixing functions provide information about the nature of mixing of the components during alloying. The negative value of the integral mixing function, ΔG^M for eutectic and some non-eutectic alloys indicates spontaneous mixing. The driving force of nucleation during solidification (ΔG_v) and the critical free energy of nucleation (ΔG^*) obtained at different undercoolings have also been highlighted. The values of radius of critical nucleus (r^*) of alloys lies within the nm scale, which suggests new dimensions of solidification processes for nano solid drug dispersions. The solid–liquid interfacial energy (σ), the grain boundary energy (σ_{gb}), and the Gibbs–Thomson coefficient (τ) of the drug alloys have been discussed. Interface morphology of the alloys follows the Jackson's surface roughness (α) theory and predicts that faceted growth ($\alpha > 2$) proceeds in all cases.

Supplemental data for this article can be accessed at www.tandfonline.com/gmcl

Keywords Critical radius; interfacial energy; phase diagram; roughness parameter; thermodynamic excess and mixing functions

Introduction

Crystal engineering has evolved in such a manner that it is now synonymous with the paradigm of supra-molecular synthesis, especially since it invokes self-assembly of existing molecules to generate a wide range of new solid forms without the need to break or form covalent bonds. This characterization is therefore well-suited for describing new, possible solid forms for pharmaceutical applications. Understanding the thermodynamic, interfacial studies and molecular phenomena that determine crystallization events has been

*Address correspondence to Vishnu Kant, Department of Chemistry, V. K. S. University, Ara, Bihar, India. E-mail: imvishnukant@gmail.com

Color versions of one or more of the figures in the article can be found online at www.tandfonline.com/gmcl.

of great pharmaceutical importance in meeting the safety and efficacy requirements of pharmaceutical products. Biological and pharmacological active chemical entities are mostly heterocyclic organic compounds. Nicotinamide is water soluble vitamin B_3, which is a nitrogen-containing heterocyclic aromatic small organic compound being a part of the vitamin B-complex. It is an anti-HIV [1], anti-M. tuberculosis [2], anti-inflammatory [3], and anti-Pellagra [4] agent. As such, nicotinamide has not been shown to produce the flushing, itching, and burning sensations of the skin as is commonly seen when large doses of niacin are administrated orally [5, 6]. In fact, a comprehensive review of nicotinamide's pharmaceutical effects came into light in 1991 as an anti-HIV agent [7], following which it was vastly popularized. Its primary activity is against susceptible forms of Streptococcus, Staphylococcus aureus, Escherichia coli, Haemophilus influenza [8], and oral anaerobes. Eutectic and non-eutectic solid dispersions [9, 10] of active pharmaceutical hydrophobic ingredients (APIs) with hydrophilic excipient Nicotinamide (NA) are important not only because of the ability to control pharmaceutical properties without changing covalent bonds, but also because they can be used in the design [11] of new materials. In recent years, advances in supramolecular engineering and chemistry have motivated more research on the design of pharmaceutical materials, especially with regard to directing molecular association of different components in the crystalline state, to form binary/ternary solid dispersions of potential interest. Pharmaceutical properties of some binary solid dispersion have also been reported [12, 13] indicating enhanced solubility, dissolution rate, hygroscopicity, and chemical stability. Indole is also a nitrogen-containing heterocyclic aromatic organic compound. It is a common component of fragrances and the precursor to many pharmaceuticals. The amino acid tryptophan is an indole derivative and is the precursor of the neurotransmitter serotonin [14]. Tryptophan is obtained from cruciferous vegetables and it has anticancer [15] properties. Eutectic mixture formation between nicotinamide based drugs and hydrophilic carriers was recently reported [16] to show a favorable reduction in the drug particle size and an increase in the dissolution rate. In the present study, nicotinamide (NA)-indole drug system was selected for measurement of its solid–liquid equilibrium phase diagram, and hence an investigation of the microstructure, thermodynamic and interfacial behavior of eutectic and non-eutectic drug alloys.

Experimental Procedure

Nicotinamide (Thomas Baker, Bombey), indole (Qualikem Fine Chemical, New Delhi) were directly taken for investigation. The melting point (experimental value) of nicotinamide, indole was found to be 128°C and 54°C respectively. The solid–liquid equilibrium data of the NA-IN system was determined by the thaw-melt method [17, 18]. Mixtures of different composition were made in glass test tubes by repeated heating followed by chilling in ice. The melting and thaw temperatures were determined in a Toshniwal melting point apparatus using a precision thermometer ($\pm$0.1°C). The heater was regulated to rise in temperature by more than 1°C every five minutes.

The heat of fusion of materials was measured by the DTA method [19, 20] using a NETZSCH Simultaneous Thermal Analyzer, STA 409 series unit. All runs were carried out with a heating rate of 2°C/min, chart speed 10 mm/min and chart speed and 100 μv/10 mV chart sensitivity. The sample weight was 5 mg for all estimations. Using benzoic acid as a standard substance, the heat of fusion of unknown compound was determined [21, 22]

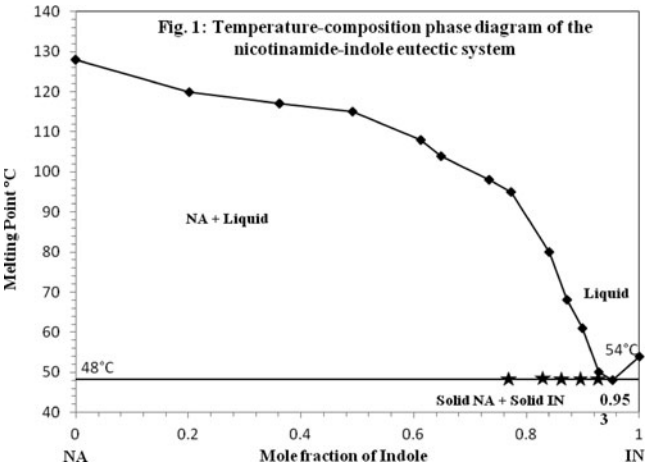

Figure 1. Temperature-composition phase diagram of the nicotinamide-indole eutectic system.

through the following equation:

$$\Delta H_x = \frac{\Delta H_s W_s A_x}{W_s A_x}$$

where ΔH_x is the heat of fusion of unknown sample, ΔH_s is the heat of fusion of standard substance, W and A are weight and peak areas, respectively, while the *x* and *s* are subscripts denoting the unknown and standard substances, respectively.

To study the microstructure of the pure components and eutectics, a small sample was taken on a well washed and dried glass slide and placed in an oven maintained at a temperature slightly above the melting point of the sample. On complete melting, a cover-slip was glided over the melt and allowed to cool. After a few minutes, the supercooled melt was nucleated by the solid of the same composition and care was taken to have unidirectional freezing. After the complete freezing, the slide was placed on the platform of an SES, DMS-01, digital microscope where observation of the different regions of the slide was carried out.

Results and Discussion

SLE Study

The solid–liquid equilibria (SLE) data of the NA-IN system, which were determined by the thaw-melt method, is reported in the form of a temperature-composition curve in Fig. 1. The NA-IN system shows the formation of a simple eutectic at a 0.953 mole fraction of IN having a melting point of 48°C. The melting point of NA (128°C) decreases on the addition of second component IN (54°C) to attain a minimum at a 0.953 mole fraction of IN, then rise to 54°C. At the eutectic temperature, two phases (a liquid phase L and two solid phases S_1 and S_2) are at equilibrium and

$$L \underset{\text{Cooling}}{\rightleftharpoons} S_1 + S_2$$

the system is invariant. The equilibrium involved among the phases are represented by the diagram

Table 1. Phase composition, melting temperature, heat of fusion (ΔH), values of entropy of fusion and entropy of fusion per unit volume (ΔSv), roughness parameter(α), interfacial energy(σ), grain boundary energy(σ_{gb}), and Gibbs–Thomson coefficient (τ) for the NA-IN system

Alloy	χ_{IN}	MP (°C)	ΔH (kJ/mol)	ΔS (J/mol/K)	α	σ (kJ/m^2)	σ_{gb} (kJ/m^2)	ΔS_v kJ/m^3/K	$\tau \times 10^6$ Km
NA		128	25.4	63.3	7.62	50.5	97.5	726	6.95
IN		54	10.6	32.4	3.90	19.3	37.2	325	5.93
E	0.953	48	11.3	35.2	4.23	20.6	39.8	355	5.81
A1	0.928	50	11.7	36.1	4.34	21.3	41.2	365	5.84
A2	0.900	61	12.1	36.2	4.35	22.1	42.8	367	6.03
A3	0.872	68	12.5	36.6	4.41	23.0	44.3	373	6.15
A4	0.841	80	13.0	36.7	4.41	23.9	46.1	375	6.35
A5	0.772	95	14.0	38.0	4.57	25.9	50.0	392	6.60
A6	0.734	98	14.5	39.2	4.71	27.0	52.2	406	6.65
A7	0.649	104	15.8	41.9	5.04	29.6	57.1	439	6.73
A8	0.613	108	16.3	42.9	5.15	30.7	59.2	452	6.79
A9	0.492	115	18.1	46.7	5.62	34.4	66.5	500	6.88
A10	0.361	117	20.1	51.4	6.19	38.5	74.4	561	6.87
A11	0.201	120	22.4	57.1	6.86	43.7	84.5	636	6.88

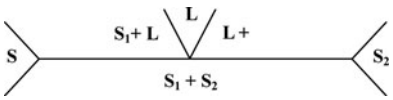

where in the eutectic region indicated by L a homogenous binary liquid solution exists, while the two solid phases exist below the horizontal line. In the case, in region located on the left side of the diagram a binary liquid and solid NA co-exist, while the region located on the right side of the diagram a binary liquid and IN co-ext equilibrium (note that S_1 is solid NA, while S_2 is solid IN).

The chemical interaction between two components in a binary system leads to an association of molecules in definite quantities. Physical as well as chemical forces are involved in the formation of eutectic and non-eutectic alloys. Thermochemical studies unfold the nature of mixing as well as nature of interactions between components of a binary mix. The values of heats of fusion of eutectic $(\Delta H)_e$ and non-eutectic alloys are calculated by the equation

$$(\Delta \mathrm{H})_e = \chi_{\mathrm{NA}} \Delta \mathrm{H}_{\mathrm{NA}} + \chi_{\mathrm{IN}} \Delta \mathrm{H}_{\mathrm{IN}} \tag{1}$$

where χ and ΔH are the mole fraction and the heat of fusion of the component indicated by the subscript, respectively. The values of heat of fusion for binary alloys of compositions A_1 through A_{11} are listed in Table 1.

Mixing and Excess Thermodynamic Functions

The integral molar free energy of mixing (ΔG^M), molar entropy of mixing (ΔS^M) and molar enthalpy of mixing (ΔH^M), and the partial thermodynamic mixing functions of the binary

Table 2. Values of integral mixing of Gibbs free energy (ΔG^M), enthalpy (ΔH^M), entropy (ΔS^M), integral excess Gibbs free energy (g^E), enthalpy (h^E), and entropy (s^E) of the eutectic for the NA-IN system

Alloy	ΔG^M kJ/mol	ΔH^M kJ/mol	ΔS^M J/mol/K	g^E kJ/mol	h^E kJ/mol	s^E kJ/mol/K
E	−0.42	−0.08	1.58	−0.08	40.9	0.125
A1	−0.48	−0.22	2.15	−0.22	−3.42	−0.009
A2	−0.22	−0.68	2.70	−0.68	−6.68	−0.019
A3	−0.09	−0.99	3.18	−0.99	−6.17	−0.018
A4	0.23	−1.51	3.64	−1.51	−6.25	−0.019
A5	0.55	−2.19	4.46	−2.19	0.82	−0.003
A6	0.54	−2.33	4.82	−2.33	36.7	0.08
A7	0.52	−2.55	5.39	−2.55	10.5	0.01
A8	0.58	−2.70	5.55	−2.70	11.3	0.01
A9	0.55	−2.79	5.76	−2.79	280	0.46
A10	0.29	−2.41	5.44	−2.41	306	0.40
A11	0.03	−1.66	4.17	−1.66	199	0.13

alloys were estimated at different compositions using the following equations

$$\Delta \mathrm{G}^M = RT(\chi_{\mathrm{NA}} \ln a_{\mathrm{NA}} + \chi_{\mathrm{IN}} \ln a_{\mathrm{IN}}) \tag{2}$$

$$\Delta S^M = -R(\chi_{\mathrm{NA}} \ln \chi_{\mathrm{NA}} + \chi_{\mathrm{IN}} \ln \chi_{\mathrm{IN}}) \tag{3}$$

$$\Delta H^M = RT(\chi_{\mathrm{NA}} \ln \gamma_{\mathrm{NA}} + \chi_{\mathrm{IN}} \ln \gamma_{\mathrm{IN}}) \tag{4}$$

$$G_i^{-M} = \mu_i^{-M} = RT \ln a_i \tag{5}$$

where $G_i^{-M}\mu_i^{-M}$ is the partial molar free energy of mixing of component i (the mixing chemical potential) in a binary mixture, γi and ai are the activity coefficient and activity of component i, respectively. The negative values [23] of the molar Gibbs free energy of mixing of alloys having compositions (A_1 to A_3, and E) that are listed in (Table 2) suggests that in these cases is spontaneous, while the positive values [24] of molar free energy of mixing of alloys of compositions (A_4–A_{11}) suggests that the mixing in all cases is non-spontaneous. The integral molar enthalpy of mixing value corresponds to that of the excess integral molar free energy of a system favoring regular solution theory.

In order to unfold the nature of the interactions between the components forming the eutectic, non-eutectic alloys and addition compound, the excess thermodynamic functions such as excess integral free energy (g^E), excess integral entropy (s^E) and excess integral enthalpy (h^E) were calculated using the following equations

$$g^E = RT(\chi_{\mathrm{NA}} \ln \gamma_{\mathrm{NA}} + \chi_{\mathrm{IN}} \ln \gamma_{\mathrm{IN}}) \tag{6}$$

$$s^E = -R\left((\chi_{\mathrm{NA}} \ln \gamma_{\mathrm{NA}} + \chi_{\mathrm{IN}} \ln \gamma_{\mathrm{IN}} + \chi_{\mathrm{NA}} T \frac{\delta \ln \gamma_{\mathrm{NA}}}{\delta T} + \chi_{\mathrm{IN}} T \frac{\delta \ln \gamma_{\mathrm{IN}}}{\delta T}\right) \tag{7}$$

$$h^E = -RT^2\left(\chi_{\mathrm{NA}} \frac{\delta \ln \gamma_{\mathrm{NA}}}{\delta T} + \chi_{\mathrm{IN}} \frac{\delta \ln \gamma_{\mathrm{IN}}}{\delta T}\right) \tag{8}$$

and the excess chemical potential or excess partial free energy of mixing is given by

$$g_i^{-E} = \mu_i^{-M} = RT \ln \gamma_i \tag{9}$$

The values of $\delta \ln \gamma i/\delta T$ can be determined from the slope of liquidus curve near the alloys formation in the phase diagram. The values of the excess thermodynamic functions of eutectic (E) are given in Table 2. The value of the excess free energy is a measure of the departure of the system from ideal behavior. The reported excess thermodynamic data substantiate the earlier conclusion of an appreciable interaction between the parent components during the formation of alloys. The negative value [25, 26] of excess free energy for all the eutectic and non-eutectic alloys indicates the possibility of a stronger association between unlike molecules. The excess entropy is a measure of the change in configurational energy due to a change in potential energy and indicates an increase in randomness.

The activity coefficient of components for the systems under investigation has been calculated from the equation [27] given below:

$$-\ln \chi_i^1 \gamma_i^1 = \frac{\Delta H_i}{R}\left(\frac{1}{T_e} - \frac{1}{T_i}\right) \tag{10}$$

where γ_i^1 is the activity coefficient of the component i in the liquid phase, ΔHi is the heat of fusion of component i at the melting point T_i, R is the gas constant, while Te is the melting temperature of alloy. Using the values of activity and activity coefficient of the components in alloys, the mixing and excess thermodynamics functions were computed.

The Gibbs-Duhem Equation

Further the partial molar quantity, activity and activity coefficient can also be determined by using the Gibbs-Duhem [28] equation

$$\sum \chi_i dz_i^{-M} = 0 \tag{11}$$

$$or\ \chi_{\mathrm{NA}} dH_{\mathrm{NA}}^{-M} + \chi_{\mathrm{IN}} dH_{\mathrm{IN}}^{-M} = 0 \tag{12}$$

$$or\ dH_{\mathrm{NA}}^{-M} = \frac{\chi_{\mathrm{IN}}}{\chi_{\mathrm{NA}}} dH_{\mathrm{IN}}^{-M} \tag{13}$$

$$or\ \left[\mathrm{H}_{\mathrm{NA}}^{-\mathrm{M}}\right]_{\chi_{\mathrm{NA}}=y} = \int_{\chi_{\mathrm{NA}}=y}^{\chi_{\mathrm{NA}}=1} \frac{\chi_{\mathrm{IN}}}{\chi_{\mathrm{NA}}} dH_{\mathrm{IN}}^{-M} \tag{14}$$

Using equation (14) a plot of H_{IN}^{-M} against $\chi_{\mathrm{IN}}/\chi_{\mathrm{NA}}$ gives the solution of the partial molar heat of mixing of a constituent NA in NA/IN alloy, while a plot of $\chi_{\mathrm{IN}}/\chi_{\mathrm{NA}}$ against $\ln \gamma_{\mathrm{IN}}$ determines the value of activity coefficient of component NA in the binary alloys.

Interfacial Studies

Interface Morphology

The science of growth has been developed on the foundation of thermodynamics, kinetics, fluid dynamics, crystal structures, and interfacial sciences. The solid-liquid interface morphology can be predicted from the value of the entropy of fusion. According to Hunt and Jackson [29], the type of growth from a binary melt depends upon a factor α, defined as:

$$\alpha = \xi \frac{\Delta H}{RT} = \xi \frac{\Delta S}{R} \tag{15}$$

where ξ is a crystallographic factor depending upon the geometry of the molecules and has a value less than or equal to one. $\Delta S/R$ (also known as Jackson's roughness parameter α) is the entropy of fusion (dimensionless) divided by the gas constant R. Where α is less than two the solid–liquid interface is atomically rough and exhibits non-faceted growth. The value of Jackson's roughness parameter ($\Delta S/R$) is given in Table 1. For the entire alloy the α value was found greater than 2, which indicates that faceted growth proceeds in all the cases.

Microstructure of Pure Components and Eutectic

The microstructure of pure components (NA and IN) and simple eutectic of the NA-IN system are shown in Fig. 2. The microstructure obtained for the eutectics are of thinly branched, interdendritic, complex regular and irregular type whereas the microstructure obtained for components are of complex and irregular type. A prediction of microstructure of eutectics can be made from Spengler's equation [30].

$$\theta = \frac{T_1 - T_E}{T_2 - T_E} \tag{16}$$

where T_1 and T_2 are the melting temperature of low-melting and high-melting components, respectively, while T_E is the eutectic temperature. Normal eutectics are formed as θ lies between 0.1 and 1.0. However, a value between 0.01 and 0.1 indicates anomalous structure, while a divorced structure prelives for θ less than 0.01. According to Podolinsky et al. [31], the surface roughness factor of one component increases or decreases under the influence of another component in a binary eutectic, as a result which the structure of eutectic

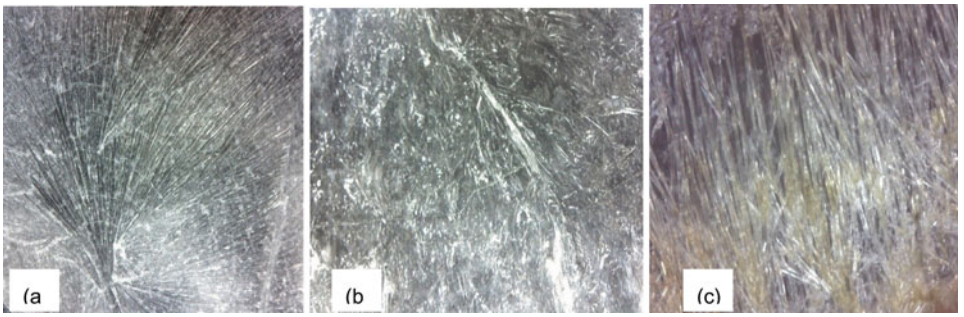

Figure 2. Microstructure of pure (a) nicotinamide ×50 (b) indole ×50, and (c) NA-IN eutectic ×230.

becomes regular. The α factor of either eutectic phase decreases under the influence of having components of opposite eutectic phases, where anomalous eutectics can be formed. The eutectic of NA-IN system having a mole fraction of 0.953 of IN grows with a thinly branched morphology. Such type of morphology is formed due to coupled stepwise steady growth of eutectic phases, and keeps going in a regular manner.

Solid–Liquid Interfacial Energy (σ)

Turnbull's empirical relationship [32] between the interfacial energy and enthalpy change provides the clue to determine the interfacial energy value for an alloy, which is expressed as:

$$\sigma = \frac{C\Delta H}{(N)^{1/3}(V_m)^{2/3}} \tag{17}$$

where the coefficient C lies between 0.33 and 0.35 for nonmetallic systems, V_m is the molar volume and N is the Avogadro's constant. The value of the solid–liquid interfacial energies of nicotinamide and indole were found to be 50.46 and 19.26 kJ m^{-2}, respectively, and the corresponding σ values for the NA-IN of alloys are listed in Table 1.

Interfacial Grain Boundary Energy (σ_{gb})

Grain boundary is the internal surface which can be understood in a very similar way to nucleation on surfaces in liquid–solid transformations. In the past, a numerical method [33] was applied to estimate the interfacial grain boundary energy (σ_{gb}) without applying the temperature gradient for the grain boundary groove shape. For an isotropic interface, there is no difference in the value of interfacial tension and interfacial energy. A considerable force is employed at the grain boundary groove in anisotropic interface. The grain boundary energy can be obtained by the equation:

$$\sigma_{gb} = 2\sigma \cos\theta \tag{18}$$

where θ is equilibrium contact angle of precipitates at the solid–liquid interface of grain boundary. The grain boundary energy could be twice the solid–liquid interfacial energy in the case where the contact angle tends to zero. The value of σ_{gb} for solid NA and IN was found to be 97.5 and 37.2 kJm^{-2} respectively and the values for all alloy compositions is given in Table 1.

The Gibbs-Thomson Coefficient (τ)

For a planar grain boundary on a planar solid–liquid interface the Gibbs-Thomson coefficient (τ) for the system can be calculated by the Gibbs-Thomson equation is expressed as

$$\tau = r\Delta T = \frac{TV_m\sigma}{\Delta H} = \frac{\sigma}{\Delta S_V} \tag{19}$$

where τ is the Gibbs–Thomson coefficient, ΔT is the dispersion in equilibrium temperature and, r is the radius of grooves of interface. The theoretical basis of determination of τ was made for equal thermal conductivities of solid and liquid phases for some transparent materials. It was also determined by the help of Gunduz and Hunt numerical method [34]

for materials having known grain boundary shape, temperature gradient in solid and the ratio of thermal conductivity of the equilibrated liquid phase to solid phase ($R = K_L/K_S$).The Gibbs–Thomson coefficient for NA and IN were estimated at 6.95×10^{-6} and 5.93×10^{-6} Km, respectively, while the corresponding values of all the alloys of different compositions are listed in Table 1.

Driving Force for Nucleation (ΔG_v)

During growth of a crystalline solid, there are changes in enthalpy, entropy and specific volume, and nonequilibrium leads to change Gibbs free energy. Thermodynamically, a metastable phase occurs in a supersaturated or super-cooled liquid. The driving force for liquid–solid transition is the difference in Gibbs energy between the two phases. Past theories of solidification process in have been discussed on the basis of the diffusion model, kinetic characteristics of nucleation and on thermodynamic features. The lateral motion of rudimentary steps in of a liquid advances a stepwise/ nonuniform surface at a low-driving force, while a continuous and uniform surface advances at sufficiently high driving force. The driving force of nucleation from liquid to solid during solidification (ΔG_V) can be determined at different undercoolings (ΔT) by using the following equation [35]

$$\Delta G_V = \Delta S_v \Delta T \tag{20}$$

This is opposed by an increase in surface free energy due to the creation of a new solid–liquid interface. By assuming that the solid phase nucleates as a small spherical cluster of radius (r) arising from random motion of atoms within the liquid. The value of ΔG_V for alloys and pure components are shown in Table 3.

Table 3. Values of volume free energy change (ΔG_v) during solidification for the NA-IN system at different undercoolings (ΔT)

	ΔG_v (kJ/m^3)→					
Alloy $\Delta T\downarrow$	1.0	1.5	2.0	2.5	3.0	3.5
E	0.355	0.532	0.710	0.887	1.07	1.24
A1	0.365	0.548	0.731	0.914	1.10	1.28
A2	0.367	0.551	0.735	0.918	1.10	1.29
A3	0.373	0.560	0.747	0.933	1.12	1.31
A4	0.375	0.563	0.751	0.939	1.13	1.31
A5	0.392	0.588	0.784	0.980	1.18	1.37
A6	0.406	0.610	0.813	1.02	1.22	1.42
A7	0.439	0.659	0.879	1.10	1.32	1.54
A8	0.452	0.677	0.903	1.13	1.36	1.58
A9	0.500	0.750	1.00	1.25	1.50	1.75
A10	0.561	0.841	1.12	1.40	1.68	1.96
A11	0.636	0.954	1.27	1.59	1.91	2.23
NA	0.726	1.09	1.45	1.82	2.18	2.54
IN	0.325	0.488	0.650	0.81	0.975	1.14

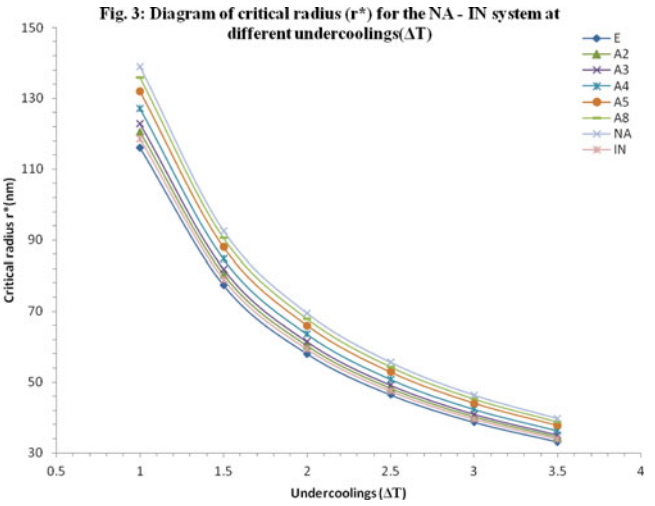

Figure 3. Diagram of critical radius (r^*) for the NA-IN system at different undercoolings (ΔT).

The effective entropy change per unit volume (ΔS_V) is calculated by the following equation

$$\Delta S_V = \frac{\Delta H}{T} \cdot \frac{1}{V_m} \tag{21}$$

where ΔH is the enthalpy change, T is the melting temperature and V_m is the molar volume of the solid phase. The entropy of fusion per unit volume (ΔS_V) for NA and IN was estimated 726 and 325 $kJK^{-1}m^{-3}$, respectively. Values of ΔS_V for the alloys are reported in Table 1.

Critical Radius (r)*

During liquid–solid transformation embryos are rapidly dispersed in an unsaturated liquid and, on undercooling, the liquid becomes saturated thus providing an embryo of a critical radius for nucleation (r^*), which can be expressed by the Chadwick relation [36]

$$r^* = \frac{2\sigma}{\Delta G_V} = \frac{2\sigma T}{\Delta H_V \Delta T} \tag{22}$$

where σ is the interfacial energy and ΔH_V is the enthalpy of fusion of the compound per unit volume, respectively. The critical sizes of the nuclii for the components and alloys were calculated at different undercoolings, and were found within the nano-scale, as is indicated in Fig. 3. It can be inferred from figure that the size of the critical nucleus decreases with an increase in the undercooling (ΔT) of the melt. The existence of embryos and a range of embryo sizes can be expected in the liquid at any temperature.

The Critical Free Energy of Nucleation (ΔG^*)

The critical radius (r^*) is a measure of the critical nucleus size and is determined by the maximum in the curve of plot of the excess free energy against (r^*) shown in the figure below.

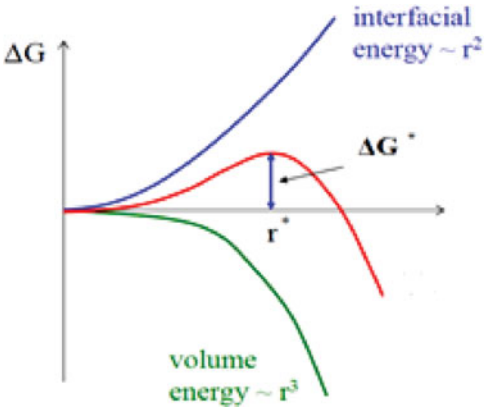

Change in the Gibbs free energy (ΔG) during nucleation plotted against r

The associated energy barrier for nucleation is responsible for forming critical nucleus, which requires a localized critical free energy/activation energy of nucleation (ΔG^*) given by [37–39]

$$\Delta G^* = \frac{16\pi\sigma^3 T^2}{3\Delta H_v^2 \Delta T^2} = \frac{16}{3}\frac{\pi\sigma^3}{\Delta G_v^2} = \frac{4}{3}\pi\sigma r*^2 \tag{23}$$

The value of ΔG^* for alloys and pure components has been found within the range of 10^{-15} to 10^{-16} J/ molecule at different undercoolings. The ΔG^* value in femto scale is not much significant at molecular level but at molar level it becomes high and suggests the formation of stable nucleus.

Conclusions

The SLE of the systems NA-IN infer the formation of simple eutectic. The mixing function suggests that in some cases mixing are spontaneous but in other it is nonspontaneous while excess functions describe the stronger association between the same components in the binary melt. Jackson's Interface roughness ($\alpha > 2$) predicts the faceted growth leads in all the eutectic and non-eutectic alloys. The eutectic of NA-IN system having mole fraction of 0.953 of IN grow with thinly branched morphology. Critical radius of all the alloys leads at different undercoolings in nano-scale. The ΔG^* value in femto scale is not much significant at molecular level but at molar level it becomes high which suggests the formation of stable nucleus.

Acknowledgment

Thanks are due to the Head of the Department of Chemistry, V. K. S. University Ara, India for providing research facilities.

References

[1] Murray, F. M., & Srinivasan, A. (1995). *Biochem. Biophys. Res. Commun.*, *210*, 954–959.
[2] Murray, F. M. (2003). *Clin. Inf. D.*, *36*, 453–460.
[3] Niren, N. M. (2006). *Cutis*, *77*, 11–16.
[4] Girgis, A. S., Hosni, H. M., & Barsoum, F. F. (2006). *Bioorg. Med. Chem.*, *14*(13), 4466–4476.
[5] Knip, M., Douek, I. F., & Moore, W. P. (2000). *Diabetologia*, *43*(11), 1337–1345.

[6] Hakozaki, T., Minwalla, L., & Zhuang, J. (2002). *Br. J. Dermatol*, *147*(1), 20–33.
[7] Yamaguchi, T., Matsumura, Y., Ishii, T., Tokuoka, Y., & Kurita, K. (2011). *Drug Dev. Res.*, *72*(3), 289–297.
[8] Sneader, W. (2005). *Drug Discovery: A History*, Wiley Press: England.
[9] Del, S. R., Lazzoi, M. R., & Vasapollo, G. (2010). *Drug Del.*, *17*(3), 130–137.
[10] Bryn, S. R., Xu, W., & Newman, A. W. (2001). *Adv. Drug Del. Rev.*, *48*, 115–136.
[11] Remenar, J. F., Morissette, S. L., Peterson, M. L., Moulton, B., MacPhee, J. M. *et al.* (2003). *J. Am. Chem. Soc.*, *125*, 8456–8457.
[12] Good, D. J., & Guez-Hornedo, N. R. (2009). *Cryst. Growth Dev.*, *9*, 2252–2264.
[13] Shiraki, K., Takata, N., Takana, R., Hayashi, Y., Terada, K. (2008). *Pharm. Res.*, *25*, 2581–2592.
[14] Nelson, D. L., & Cox, M. M. (2005). *Principles of Biochemistry*, 4th edn., W. H. Freeman: New York.
[15] Ahamad, A., Sakr, W. A., & Rahman, K. M. (2010). *Curr. Drug Targets*, *11*(6), 652–666.
[16] Terauchi, H., Tanitame, A., Tada, K., Nakamura, K., Seto, Y., *et al.* (1997). *Med. Chem.*, *40*, 313–321.
[17] Dwivedy, Y., Kant, S., Rai, U. S., & Rai, R. N. (2011). *J. Fluoresc.*, *21*, 1255–1263.
[18] Agrwal, T., Gupta, P., Das, S. S., Gupta, A., & Singh, N. B. (2010). *J. Chem. Engg. Data*, *55*, 4206–4210.
[19] Shekhar, H., & Kant, V. (2012). *Int. J. Pharm. Tech. & Res.*, *4*(4), 1486–1497.
[20] Shekhar, H., & Salim, S. S. (2011). *J. Nat. Acad. Sci. Lett.*, *34*, 117–125.
[21] Krajewska-Cizio, A. (1990). *Thermochimica Acta*, *158*, 317–325.
[22] Sangester, J. (1994). *J. Phy. Chem. Ref. Data*, *23*, 295–317.
[23] Sharma, B. L., Tandon, S., & Gupta, S. (2009). *Cryst. Res. Technol*, *44*, 258–268.
[24] Nieto, R., Gonozalez, M. C., & Herrero, F. (1999). *Am. J. Phys.*, *67*, 1096–1099.
[25] Shamsuddin, M., Singh, S. B., & Nasar, A. (1998). *Thermochemica Acta*, *316*, 11–19.
[26] Shekhar, H., Pandey, K. B., & Kant, V. (2012). *Int. J. Chem.*, *1*(2), 257–263.
[27] Shekhar, H., & Kant, V. (2013). *Asian J. Chem.*, *25* (5), 2441–2446.
[28] Rai, U. S., & Shekhar, H. (1994). *Cryst. Res. Technol*, *29*, 533–542.
[29] Hunt, J. D., & Jackson, K. A. (1966). *Trans. Metall. Soc. AIME*, *236*, 843–852.
[30] Spengler, H., & Metallk, Z. (1957). *Trans. Metall. Soc. AIME*, *11*, 384–388.
[31] Podolinsky, V. V., & Drykin, V. G. (1983). *J. Cryst. Growth*, *62*(3), 532–538.
[32] Turnbull, D. (1950). *J. Chem. Phys.*, *18*, 768–769.
[33] Bayram, U., Aksöz, S., & Maraşlı, N. (2013). *Thermochemica Acta*, *554*, 48–53.
[34] Gunduz, M., & Hunt, J. D. (1989). *Acta Metall.*, *37*, 1839–1845.
[35] Hunt, J. D., & Lu, S. Z. (1994). *Hand Book of Crystal Growth*, edt. DTJ Hurle, Elsevier: Amsterdam, pp. 112.
[36] Chadwick, G. A. (1972). *Metallography of Phase Transformation*, Butterworths: London, pp. 6.
[37] Wilcox, W. R. (1974). *J. Cryst. growth*, *26*, 153–154.
[38] Bai, X.-M., & Li, M. (2006). *J. Chem. Phys*., *124*, 124707–124712.
[39] Nicholson, R. B., & Davies, G. J. (1971). *Development of Microstructure: In structural characteristics of materials*, ed. H. M. Finniston, Elsevier Publishing Co. Ltd.: Amsterdam.